RIS-Aided Short-Packet Communication with Imperfect CSI: Average Block Error Rate Analysis

1st Si-Phu Le
Department of Telecommunications
VSB – Technical University of Ostrava
Ostrava, Czech Republic
phu.le.si@vsb.cz

2nd Hong-Nhu Nguyen
Faculty of Electronics and Telecommunications
Saigon University
Ho Chi Minh City, Vietnam
nhu.nh@sgu.edu.vn

3rd Dat-Tan Huynh
Department of Admissions
Nam Sai Gon Polytechnic College
Ho Chi Minh City, Vietnam
tandat@nsg.edu.vn

4th Giovanni A. Salvatore
Department of Molecular Systems and Nanosystems
Ca' Foscari - University of Venice
Mestre, (VE), Italy
giovanni.salvatore@unive.it

5th Erik Chromy
Faculty of Informatics
Pan-European University
Bratislava, Slovakia
erik.chromy@paneurouni.com

6th Miroslav Voznak
Department of Telecommunications
VSB – Technical University of Ostrava
Ostrava, Czech Republic
miroslav.voznak@vsb.cz

***Abstract*—In this research, we examine the average block error rate (BLER) of a short-packet communications (SPC) system with imperfect channel state information (CSI) that is supported by a reconfigurable intelligent surface (RIS). To be more precise, we derive the cumulative distribution function (CDF) and the probability density functions (PDF) of the end-to-end signal-to-interference-plus-noise ratio (SINR) taking into account the imperfect CSI from the RIS to the destination. Closed-form formulas for average BLER, throughput, goodput, latency, and dependability are provided. In a high transmit signal-to-noise ratio (SNR), we construct not only the closed-form formulae for the average approximate BLER of the user but also the average asymptotic BLER. Furthermore, numerical outcomes show that the generated closed-form equations agree with the outcomes of the simulations. The simulation results also show how the blocklength and number of RIS elements affect the BLER performance of the system.**

***Index Terms*—Block error rate (BLER), Reconfigurable Intelligent Surface (RIS), imperfect channel state information (CSI), short-packet communication (SPC).**

I. Introduction

Reconfigurable intelligent surfaces (RIS) are energy-efficient communication technologies that utilize metasurfaces, radio frequency micro-electro-mechanical systems (MEMS), and other related technologies [1]. By adjusting phase shifts, RIS can modify wireless propagation environments without a power source or complex signal processing [2] with the radio propagation environment to amplify desirable signals and/or weaken unwanted ones [3]. Recent system performance analysis has focused on using the K_G [4] and the non-central chi-square (NCCS) distribution [5] to approximate the signal-to-noise ratio (SNR) distribution from the RIS to receivers. Additionally, when there are few passive reflecting components, the K_G distribution is more accurate than the NCCS distribution in [6]. In order to use ultra-reliable and low-latency communications (uRLLC) service for Internet of Things (IoT) applications [7], or short-packet communications (SPC) by use of finite blocklength coding (FBC), which, when compared to its usual infinite blocklength equivalent, may greatly reduce the physical layer transmission latency [8] has been proposed as a critical technology. Previous study [9] introduced a unique performance parameter of the block error rate (BLER) to measure and create the SPC networks. SPC research in wireless networks has received great interest in [10]. The secure throughput and blocklength optimization of a three-node wiretap single-input multiple-output (SIMO) channel in a Rayleigh fading environment were discussed in [11], respectively, for situations involving a single eavesdropper and a multiple eavesdropper. Furthermore, in [12], the authors examined user dependability, latency, and BLER system performances in wirelessly powered cognitive SPC networks. RIS-aided SPC networks have been thoroughly examined in a variety of wireless communication scenarios in [13] for addressing the formulas for system average decoding error probability and data rate, taking into account the RIS-supported SPC uRLLC networks. But perfect channel state information (CSI) is not discussed in depth due to insufficient radio resources at the RIS. Previous studies have focused on beamforming design for RIS-aided systems with inadequate CSI. [14]. Nevertheless, there aren't many studies discussing how CSI errors affect RIS-assisted SPC system performance. Inspired by the above observations, we obtain the average BLER's closed-form expressions, the BLERs' approximate expressions in closed form, and the asymptotic BLERs in a high signal-to-noise ratio (SNR) regime. The analytical BLER expressions are verified through system throughput

The research was co-funded by the European Union (EU) within the REFRESH project – Research Excellence For REgion Sustainability and High-tech Industries ID No. CZ.10.03.01/00/22_003/0000048 of the European Just Transition Fund, and also supported by the Ministry of Education, Youth and Sports of the Czech Republic (MEYS CZ) within a Student Grant Competition in the VSB – Technical University of Ostrava under project ID No. SGS SP2024/061.

and Monte Carlo simulations for a RIS-assisted SPC wireless system with imperfect CSI. There is a noticeable decline in performance and a performance floor as compared to the ideal CSI equivalent. It is observed that our work differs from that of [3], where the receiver in question is the RIS.

Notation: $\mathbb{E}\{.\}$ is the Expectation operator; $K_n(.)$ is so-called the Bessel function; $G_{p,q}^{m,n}(.)$ is so-called the Meijer G-function; $\Gamma(.)$ denote the gamma function; $\mathcal{Q}(.)$ is the Gaussian Q-function; $\mathcal{O}(.)$ is the higher order terms; $W_{p,q}(.)$ is so-called the Whittaker function; $\mathcal{H}_{p,q:u,v:e,f}^{m,n:s,t:i,j}(\cdot)$ represents the extended generalized bivariate Fox H-function; the probability density function (PDF) and the cumulative distribution function (CDF) of a random variable X are represented as $F_X(.)$ and $f_X(.)$.

II. System Model

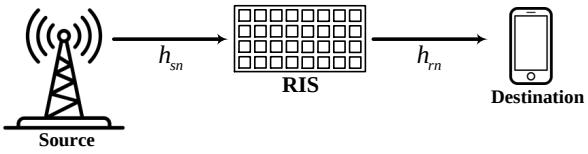

Fig. 1. An exemplification of an SPC system with RIS assistance.

We consider a RIS-aided single-input single-output (SISO) SPC system as shown in Fig. 1, which includes a source (S), a destination (D), and a RIS (with N passive reflecting components). We assume S and D each have a single antenna. We presume that impediments prevent a straight connection between S and D. The RIS is configured with optimal phase shifts to reflect the incoming signals to D after receiving signals from S.

The channel that fades from S to the RIS's nth reflecting element, $\forall n \in \mathcal{N}$ with $\mathcal{N} = [1, 2, \ldots, N]$, is indicated in the system as

$$h_{sn} = |h_{sn}| e^{j\angle h_{sn}}, \tag{1}$$

where $\angle h_{sn}$ and $|h_{sn}|$ are the phase and amplitude of the h_{sn} channel, respectively. The channel that fades from the nth reflecting element of the RIS to D, $n \in \mathcal{N}$, is indicated by

$$h_{rn} = |h_{rn}| e^{j\angle h_{rn}}, \tag{2}$$

where $\angle h_{rn}$ and $|h_{rn}|$ are the phase and amplitude of the h_{rn} channel, we assumed that h_{sn} and h_{rn} are independently and identically distributed (i.i.d.) circularly symmetric complex Gaussian (CSCG) random variables with a mean of zero and specified variances $d_{sn}^{-\alpha}$ and $d_{rn}^{-\alpha}$, in which $alpha$ is the path loss factor, d_{sn} and d_{rn} are S-RIS and RIS-D link distances ($h_{sn} \sim \mathcal{CN}(0, d_{sn}^{-\alpha}), h_{rn} \sim \mathcal{CN}(0, d_{rn}^{-\alpha})$).

Base on [15], we assume that the S-RIS connection is perfect[1], but the RIS-D link is flawed owing to channel estimate error and restricted feedback. The generally used equation is employed in this letter to simulate the consequences of imperfect CSI [16]–[18]

$$h_{rn} = \tilde{h}_{rn}\chi + \Delta h_{rn}\sqrt{1-\chi^2}, \tag{3}$$

where the variables $\tilde{h}_{rn}$ and Δh_{rn} are complex Gaussian random variables with mean zero and variance $d_{rn}^{-\alpha}$. The ideal channel is denoted by h_{rn}, the known channel estimation at D is represented by $\tilde{h}_{rn}$, and the correlation coefficient between h_{rn} and $\tilde{h}_{rn}$ is χ.

We set P_S to represent the transmit power, the received signal at D may be written as

$$\begin{aligned}\bar{y} =& \chi\sqrt{P_S}\sum_{n=1}^{N} h_{sn}\nu_n\tilde{h}_{rn}x + \sqrt{P_S(1-\chi^2)} \\ &\times \sum_{n=1}^{N} h_{sn}\nu_n\Delta h_{rn}x + \omega,\end{aligned} \tag{4}$$

where the intended signal is the first term and the interference brought on by the malfunctioning CSI is the second term. ω is the additive white Gaussian noise (AWGN) with a mean zero and variance σ_D^2. The transmit signal of S with unit energy x with $\mathbb{E}\left\{|x|^2\right\} = 1$. The phase and reflection coefficient generated by the RIS's nth reflector are denoted by $\nu_n = \beta_n e^{j\theta_n}$ in equation (4), where $\beta_n = 1$ and θ_n, $n \in \mathcal{N}$. Thus, for x decoding, the signal-to-interference-plus-noise ratio (SINR) at D is provided by

$$\bar{\gamma}_D = \frac{\chi^2 P_S\left|\sum_{n=1}^{N} h_{sn}\tilde{h}_{rn}e^{j\theta_n}\right|^2}{(1-\chi^2)\, d_{rd}^{-\alpha} P_S\left|\sum_{n=1}^{N} h_{sn}e^{j\theta_n}\right|^2 + \sigma_D^2}. \tag{5}$$

As in [19], by establishing the phases[2] $\theta_n = -\angle h_{sn} - \angle\tilde{h}_{rn}$, $\forall n \in \mathcal{N}$. The maximum $\bar{\gamma}_D$ is as follows:

$$\bar{\gamma}_D = \frac{\chi^2\rho_S\left|\sum_{n=1}^{N}|h_{sn}|\left|\tilde{h}_{rn}\right|\right|^2}{(1-\chi^2)\, d_{rn}^{-\alpha}\rho_S\left|\sum_{n=1}^{N} h_{sn}e^{j\theta_n}\right|^2 + 1} = \frac{\chi^2\rho_S\mathcal{A}}{\rho_S\mathcal{B}+1}, \tag{6}$$

where $\rho_S = P_S/\sigma_D^2$ is the transmit signal-to-noise radio (SNR), $\mathcal{A} = \left|\sum_{n=1}^{N}|h_{sn}|\left|\tilde{h}_{rn}\right|\right|^2$ and $\mathcal{B} = \left(1-\chi^2\right) d_{rn}^{-\alpha}\left|\sum_{n=1}^{N} h_{sn}e^{j\theta_n}\right|^2$.

In [6], a very accurate closed-form approximation to the distribution of $\mathcal{A}$ for arbitrary values of N is proposed, based on the small argument approximation (SAA) approach. For instance, a squared K_G distribution with the following values

[1]In reality, S (such as a base station or access point) and RIS are often placed in fixed locations. As a result, by computing the angles of arrival and departure, which fluctuate slowly, the S-RIS link may be precisely determined [15].

[2]This letter's phase setting differs from that of [20], which is connected to beamforming, as beamforming cannot be implemented assuming a transmitter with a single antenna.

may be used to approximate the PDF and CDF of $\mathcal{A}$ i given by

$$f_{\mathcal{A}}(x) \simeq \frac{2\Xi^{k_w+m_w} x^{\left(\frac{k_w+m_w-2}{2}\right)}}{\Gamma(k_w)\Gamma(m_w)} K_{k_w-m_w}\left(2\Xi\sqrt{x}\right), \quad (7a)$$

$$F_{\mathcal{A}}(x) \simeq \frac{1}{\Gamma(k_w)\Gamma(m_w)} G_{1,3}^{2,1}\left(\Xi^2 x \,\middle|\, \begin{matrix} 1 \\ k_w, m_w, 0 \end{matrix}\right), \quad (7b)$$

where $G_{p,q}^{m,n}(.)$ is so-called the Meijer G-function, $\Gamma(.)$ denote the gamma function, $K_q(.)$ is the modified q-order Bessel function of the second kind, $m_w = \frac{-b-\sqrt{b^2-4ac}}{2a}$ and $k_w = \frac{-b+\sqrt{b^2-4ac}}{2a}$ are the shaping parameters, $\Xi = \sqrt{k_w m_w/\lambda_w}$ in which $\lambda_w = \mu_X(2)$ denote the mean of $\mathcal{A}$. Additionally, describe the kth instant of $\mathcal{A}$ as

$$\mu_{\mathcal{A}}(k) = \sum_{j_1=0}^{k} \sum_{j_2=0}^{j_1} \cdots \sum_{j_{N-1}=0}^{j_{N-2}} \binom{k}{j_1}\binom{j_1}{j_2}\cdots\binom{j_{N-2}}{j_{N-1}} \times \mu_{\mathcal{A}_1}(k-j_1)\,\mu_{\mathcal{A}_2}(j_1-j_2)\cdots\mu_{\mathcal{A}_{N-1}}(j_{N-1}), \quad (8)$$

where $\mu_{\mathcal{A}_n}(k) = (d_{sr}d_{rn})^{-0.5k\alpha}[\Gamma(1+0.5k)]^2$ is the kth moment of $\mathcal{A}_n = |h_{sn}|\left|\tilde{h}_{rn}\right|$. It is possible to define the parameters a, b, and c as

$$a = \mu_{\mathcal{A}}(6)\,\mu_{\mathcal{A}}(2) - 2\mu_{\mathcal{A}}(4)^2 + \mu_{\mathcal{A}}(2)^2\mu_{\mathcal{A}}(4), \quad (9a)$$

$$b = \mu_{\mathcal{A}}(6)\,\mu_{\mathcal{A}}(2) + 3\mu_{\mathcal{A}}(2)^2\mu_{\mathcal{A}}(4) - 4\mu_{\mathcal{A}}(4)^2, \quad (9b)$$

$$c = 2\mu_{\mathcal{A}}(2)^2\mu_{\mathcal{A}}(4). \quad (9c)$$

We obtain $h_{sn}e^{j\theta_n} = |h_{sn}|\,e^{j\angle\tilde{h}_{rn}} \sim \mathcal{CN}(0, d_{rn}^{-\alpha})$ by using the circular symmetry of h_{sn}. Consequently, the PDF of $\mathcal{B}$ may be written as

$$f_{\mathcal{B}}(x) = \tfrac{1}{\delta}e^{-\frac{x}{\delta}} \quad , x > 0 \quad (10)$$

where $\delta = N\left(1-\chi^2\right)/(d_{sn}d_{rn})^{\alpha}$. From (6), the formula for the CDF of $\bar{\gamma}_D$ is

$$F_{\bar{\gamma}_D}(z) = \Pr\left(\frac{\chi^2\mathcal{A}}{1/\rho_S+\mathcal{B}} < z\right) = \int_0^{\infty}\int_0^{\frac{z}{\chi^2}\left(\frac{1}{\rho_S}+y\right)} f_{\mathcal{A}}(x) f_{\mathcal{B}}(y)\,dxdy \quad (11)$$

Unfortunately, because of the shift $1/\rho_S$ in the upper limit of the inner integral, it is challenging, if not impossible, to find the precise closed-form equation for (11). Therefore, the quantity $\mathcal{B}+1/\rho_S$ in equation (6) may be roughly represented as a Gamma distributed random variable [21], which we will refer to as $\tilde{\mathcal{B}}$. Its PDF is as follows

$$f_{\tilde{\mathcal{B}}}(y) = \Gamma(\varphi)^{-1}\xi^{\varphi}y^{\varphi-1}e^{-\xi y} \quad , y > 0 \quad (12)$$

where the scale and shape parameters are indicated by ξ and φ. The moment-matching approach is employed in the parameter computation. Specifically, by matching $\mathcal{B}+1/\rho_S$ and $\tilde{\mathcal{B}}$'s first and second moments, i.e.,

$$\begin{cases} \delta + 1/\rho_S = \varphi/\xi \\ 2\delta^2 + 2\delta/\rho_S + 1/\rho_S^2 = \left(\varphi^2+\varphi\right)/\xi^2 \end{cases} \quad (13)$$

in which $\xi = \delta^{-1}\left[1+(\delta\rho_S)^{-1}\right]$ and $\varphi = \left[1+(\delta\rho_S)^{-1}\right]^2$. This approximation eliminates the shift $1/\rho_S$ in the top limit of the inner integral in (11) as seen in (14). When (12) is substituted with (11), the CDF of $\bar{\gamma}_D$ is given as

$$F_{\bar{\gamma}_D}(z) = \Pr\left(\frac{\chi^2\mathcal{A}}{\tilde{\mathcal{B}}} < z\right) = \int_0^{\infty}\int_0^{\frac{zy}{\chi^2}} f_{\mathcal{A}}(x) f_{\tilde{\mathcal{B}}}(y)\,dxdy. \quad (14)$$

The approximation used at $\tilde{\mathcal{B}}$ causes the shift $1/\rho_S$ in the upper limit of the inner integral to be eliminated. By changing (7a) and (12) in (14), we obtain

$$F_{\bar{\gamma}_D}(z) = \frac{\phi}{\xi^{-\varphi}}\int_0^{\infty} y^{\varphi-1}e^{-\xi y} G_{1,3}^{2,1}\left(\frac{\Xi^2}{\chi^2}zy \,\middle|\, \begin{matrix} 1 \\ k_w, m_w, 0 \end{matrix}\right) dy, \quad (15)$$

where $\phi = \frac{1}{\Gamma(k_w)\Gamma(\varphi)\Gamma(m_w)}$.

With the aid of [22, Eq. (7.813.1)], then following a few simple procedures, the CDF of $\bar{\gamma}_D$ is represented as

$$F_{\bar{\gamma}_D}(z) = \phi G_{2,3}^{2,2}\left(\frac{\Xi^2 z}{\chi^2\xi} \,\middle|\, \begin{matrix} 1-\varphi, 1 \\ k_w, m_w, 0 \end{matrix}\right). \quad (16)$$

The PDF of $\bar{\gamma}_D$ is derived by calculating the partial derivativwith regard to z and using [23, Eq. (8.2.2.30)] and [22, Eq. (9.31.1)], we have

$$f_{\bar{\gamma}_D}(z) = \frac{\phi}{z} G_{1,2}^{2,1}\left(\frac{\Xi^2 z}{\chi^2\xi} \,\middle|\, \begin{matrix} 1-\varphi \\ k_w, m_w \end{matrix}\right). \quad (17)$$

III. PERFORMANCE ANALYSIS

In this part, we analyze the average BLER in the RIS-aided short-packet system under consideration. In bit per channel usage (BPCU), the maximum attainable rate (MAR) for x at D is stated as

$$\bar{\mathcal{R}}_D = \mathcal{C}(\bar{\gamma}_D) - \mathcal{Q}^{-1}(\varepsilon_D)\sqrt{\frac{\mathcal{V}(\bar{\gamma}_D)}{\mathcal{L}}} + \mathcal{O}\left(\frac{\log_2\mathcal{L}}{\mathcal{L}}\right), \quad (18)$$

where $\mathcal{L}$ and ε_D are the transmit blocklength and BLER, respectively, for D recovering x. Shannon capacity is denoted by $\mathcal{C}(\bar{\gamma}_D) = \log_2(1+\bar{\gamma}_D)$, and channel dispersion is denoted by $\mathcal{V}(\bar{\gamma}_D) = (\log_2 e)^2\left(1-1\Big/(1+\bar{\gamma}_D)^2\right)$. $\mathcal{Q}^{-1}(.)$ is the Gaussian Q-function's inverse, and $\mathcal{O}(\log_2\mathcal{L}/\mathcal{L})$ represents the remaining components of order $\log_2\mathcal{L}/\mathcal{L}$, which is negligible if $\mathcal{L} \geq 100$ holds.

The instantaneous BLER ε_D is estimated from (18), for a given transmission rate $\mathcal{R} \triangleq \mathcal{T}/\mathcal{L}$ at D in which contains data amount $\mathcal{T}$ (bits) with blocklength $\mathcal{L}$, by omitting the high order elements as

$$\varepsilon_D(\bar{\gamma}_D) \approx \mathcal{Q}\left(\frac{\mathcal{C}(\bar{\gamma}_D) - \mathcal{R}}{\sqrt{\mathcal{V}(\bar{\gamma}_D)/\mathcal{L}}}\right). \quad (19)$$

Next, the average BLER $\bar{\varepsilon}_D$ is calculated as

$$\bar{\varepsilon}_D = E\{\varepsilon_D\} = \int_0^{\infty} \varepsilon_D(x)\, f_{\bar{\gamma}_D}(x)dx. \quad (20)$$

Because of the intricacy of the Q-function, it is quite challenging to obtain an accurate closed-form formula for $\bar{\varepsilon}_D$

$$\Lambda(x,y)=\mathcal{H}_{1,1:2,3:1,1}^{0,1:2,2:0,1}\left(\begin{array}{c|c|c|c} (0;1,1) & (1-\varphi,1);(1,1) & (1,1) & \\ (-1;1,1) & (k_w,1);(m_w,1);(0,1) & (0,1) & |x,y \end{array}\right). \tag{25}$$

from (19) and (20). To simplify this situation, we utilize the linear approximation of the Q-function as [24]

$$\mathcal{W}(\bar{\gamma}_D)=\begin{cases} 1, & \bar{\gamma}_D \le \varpi \\ 0.5-\varsigma(\bar{\gamma}_D-\gamma_{th}), & \varpi \le \bar{\gamma}_D < \tau \\ 0, & \bar{\gamma}_D > \varpi \end{cases} \tag{21}$$

where $\varsigma=\sqrt{2\pi\left(2^{2\mathcal{R}}-1\right)/\mathcal{L}}$, $\gamma_{th}=2^{\mathcal{R}}-1$, $\varpi=\gamma_{th}-1/2\varsigma$ and $\tau=\gamma_{th}+1/2\varsigma$.

By plugging (21) for (20) and using the integration by parts, $\bar{\varepsilon}_D$ may be re-expressed as

$$\bar{\varepsilon}_D=\varsigma\int_{\varpi}^{\tau}F_{\bar{\gamma}_D}(x)dx. \tag{22}$$

A. Average BLER Analysis

Substituting (16) into (22), the average BLER of D can be rewritten as

$$\bar{\varepsilon}_D=\varsigma\phi\int_{\varpi}^{\tau}G_{2,3}^{2,2}\left(\frac{\Xi^2}{\chi^2\xi}x\,\middle|\,\begin{array}{c}1-\varphi,1\\ k_w,m_w,0\end{array}\right)dx. \tag{23}$$

Proposition 1: The BLER of decoding x at D is given by

$$\bar{\varepsilon}_D=\varsigma\phi\varpi\Lambda\left(\frac{\varpi\Xi^2}{\chi^2\xi},\frac{\varpi}{\tau}\right), \tag{24}$$

where $\Lambda(x,y)$ is shown on the top page and $\mathcal{H}_{p,q:u,v:e,f}^{m,n:s,t:i,j}(\cdot)$ represents the extended generalized bivariate Fox H-function (EGBFHF) in [25].

Proof: See Appendix A. ∎

The extended generalized bivariate Fox H-function in (24) on the other hand, results in a high amount of processing complexity. To overcome this barrier, we use the midpoint approximation approach to find $\bar{\varepsilon}_D$ in the equation below. Because the difference between τ and ϖ in (23) is so small [26, Eq. (11)] $\bar{\varepsilon}_D$ can be further simplified by

$$\bar{\varepsilon}_D^{App}=\frac{\varsigma\phi}{P}\sum_{p=1}^{P}G_{2,3}^{2,2}\left(\frac{\Xi^2\kappa(p)}{\chi^2\xi}\,\middle|\,\begin{array}{c}1-\varphi,1\\ k_w,m_w,0\end{array}\right), \tag{26}$$

where $\kappa(p)=\varpi+(2p-1)(\tau-\varpi)/2P$ and the parameter P denotes the complexity-accuracy trade-off parameter.

B. Average Asymptotic BLER Analysis

As $\rho_S\to\infty$, according to (6), we have $\bar{\gamma}_D^{\infty}\approx\frac{\chi^2\mathcal{A}}{\mathcal{B}}$. Therefore, we can deduce that CDF at High SNR is provided by

$$F_{\bar{\gamma}_D^{\infty}}(z)=\Pr\left(\bar{\gamma}_D^{\infty}<z\right)=\int_0^{\infty}\int_0^{\frac{zy}{\chi^2}}f_{\mathcal{A}}(x)f_{\mathcal{B}}(y)\,dxdy. \tag{27}$$

After performing a few mathematical operations and switching the integral's order, we obtain

$$\begin{aligned}F_{\bar{\gamma}_D^{\infty}}(z)=&\frac{2\Xi^{k_w+m_w}}{\Gamma(k_w)\Gamma(m_w)}\int_0^{\infty}e^{-\frac{\chi^2 x}{\delta z}}x^{\left(\frac{k_w+m_w-2}{2}\right)}\\ &\times K_{k_w-m_w}\left(2\Xi\sqrt{x}\right)dx.\end{aligned} \tag{28}$$

The approximate CDF of $\bar{\gamma}_D^{\infty}$ is expressed using [22, Eq. (6.631.3)] as

$$\begin{aligned}F_{\bar{\gamma}_D^{\infty}}(z)=&e^{\frac{\delta\Xi^2 z}{2\chi^2}}\left(\frac{\delta\Xi^2 z}{\chi^2}\right)^{\frac{k_w+m_w-2}{2}}\\ &\times W_{-\frac{k_w+m_w-1}{2},\frac{k_w+m_w}{2}}\left(\frac{\delta\Xi^2 z}{\chi^2}\right),\end{aligned} \tag{29}$$

where $W_{p,q}(.)$ is so-called the Whittaker function.

We have $\bar{\varepsilon}_D$ may be estimated from (22) using the first-order Riemann integral approximation as

$$\bar{\varepsilon}_D^{Asy}\approx F_{\bar{\gamma}_D^{\infty}}(\gamma_{th}). \tag{30}$$

By substituting (29) into (30), the average asymptotic BLER at D is

$$\begin{aligned}\bar{\varepsilon}_D^{Asy}\to\, &e^{\frac{\delta\Xi^2\gamma_{th}}{2\chi^2}}\left(\frac{\delta\Xi^2\gamma_{th}}{\chi^2}\right)^{\frac{k_w+m_w-2}{2}}\\ &\times W_{-\frac{k_w+m_w-1}{2},\frac{k_w+m_w}{2}}\left(\frac{\delta\Xi^2\gamma_{th}}{\chi^2}\right).\end{aligned} \tag{31}$$

C. System Throughput and Goodput Analysis

In short-packet communication, characterized by its focus on minimizing latency and maximizing reliability, the length of the transmitted block is frequently defined in the form of small packets. Consequently, the probability of packet error at the receiver becomes significant. In examining the impact of non-zero error probability on the decoding of the signal for the user, we present two performance metrics: throughput and goodput. These metrics serve to underscore the benefits of the proposed system regarding delay reduction in comparison to the orthogonal equivalent. The throughput measured in nats per channel usage (npcu) serves as the criterion for assessing effective communication at a constant channel coding rate, $\bar{\mathcal{R}}_D$. Mathematically, the throughput is derived by multiplying $\bar{\mathcal{R}}_D$ by the end-to-end decoding packets at user $(1-\bar{\varepsilon}_D)$. In contrast to throughput, goodput in npcu is characterized as a metric that assesses the effective communication rate when frames or data are successfully transmitted across the network, while considering the overall utilization of the channel, including both training and data. In order to evaluate goodput, it is necessary to determine the number of channels utilized for actual data L_d and training L_t. Mathematically, goodput is calculated as the ratio of effective channel samples to the total number of channel uses L_{tot} multiplied by $\bar{\mathcal{R}}_D$ and $(1-\bar{\varepsilon}_D)$.

Then, the total system throughput, represented by $\mathbb{T}$, and total system goodput, designated by $\mathbb{G}$, may be evaluated from [27] and [28], by

$$\mathbb{T} = (1 - \bar{\varepsilon}_D)\,\mathcal{R}, \tag{32a}$$

$$\mathbb{G} = \left(1 - \frac{L_t}{L_{tot}}\right)\mathbb{T}. \tag{32b}$$

where L_t is the channel uses for the training communication and L_d is the channel uses for data transmission and L_{tot} is the total number of channel uses per each time-slot in which $L_{tot} = L_t + L_d$.

The analysis of (32a) and (32b) provides valuable insights, particularly about how increasing the specified constant rate $\bar{\mathcal{R}}_D$ leads to increased system throughput. Recall that $\bar{\mathcal{R}}_D$ is likewise controlled by the ratio of the amount of user bits of information $\mathcal{T}$ to L_d. Consequently, we may proceed with approach enhancements: If $\mathcal{T} < L_d$, increase $\mathcal{T}$; otherwise, decrease L_d. Meanwhile, when the total number of channels used is fixed, higher system goodput is dominated by both $\bar{\mathcal{R}}_D$ and L_t. In such instances, there is a vital relationship between managing $\mathcal{T}$ and L_t. Smaller L_t yields larger L_d. Thus, additional user information is necessary.

D. Latency and Reliability Analysis

Two important factors for assessing real-time capability in the interactive connection of devices for developing IoT systems are latency and dependability, in addition to good throughput and throughput. According to [29], URLLC applications that adhere to 3GPP standards must generally ensure that a single 32-byte packet is sent with less than 99.99% of the time, all within a user plane latency of 1 ms. Therefore, it is required to ascertain the transmission latency and dependability in order to gauge the quality of the system under consideration with such URLLC standards.

The average time to correctly transport and decode a packet across the radio interface is known as the physical layer's latency. Reliability, on the other hand, is the likelihood that $\mathcal{T}$ information bits will be successfully sent across a specific channel quality for the anticipated user plane time. It is important to remember that reduced reliability and higher latency for higher layers may result from the physical layer's cause of failure, which might be packet loss, decoding mistakes, residual errors, or late packet reception. Based on the definitions given above, we may infer that $\tilde{\mathcal{T}}$ is the fixed period required for successfully decoding packets sent from the source to the consumers. Based on the end-to-end BLER, the latency, indicated by $\tilde{\mathcal{L}}$, in milliseconds (ms) and reliability, denoted by $\tilde{\mathcal{R}}$, in percent (%) for each user, may be assessed from [30], [12], respectively, by

$$\tilde{\mathcal{L}} = \frac{2L_d\tilde{\mathcal{T}}}{1 - \bar{\varepsilon}_D}, \tag{33a}$$

$$\tilde{\mathcal{R}} = 100 \times (1 - \bar{\varepsilon}_D)\,. \tag{33b}$$

TABLE I
MAIN SYSTEM PARAMETERS

Monte Carlo simulations	10^7 iterations
Total reflecting elements	$N = 8$
Bandwidth	$\mathrm{BW} = 10$ [MHz]
Noise figure	$\mathrm{NF} = 10$ [dBm]
Thermal noise power density	$N_0 = -174$ [dBm/Hz]
Number of information bits	$\eta = 80$ [bits]
Blocklength	$\mathcal{L} = 200$
The distance from S to RIS	$d_{sr} = 60$ [m]
The distance from RIS to D	$d_{rd} = 80$ [m]
The path loss exponent	$\alpha = 3$
Channel uses for data transmission	$L_d = 300$
Channel uses for data transmission	$L_t = 100$

IV. NUMERICAL RESULTS

In this section, we assessed the performance of the derived theoretical expression and produced numerical results to validate the analytical expression. The main parameters are listed in Table 1. Additionally, the equivalent noise power at D was calculated as $\omega_D^2 = N_0 + 10\log(\mathrm{BW}) + \mathrm{NF}$ [dBm] in [31]. Our code's technological contribution is the use of symbolic calculations in Matlab, which allowed us to achieve very accurate results. In addition, the complexity accuracy trade-off parameter is selected as $P = 5$ to yield a close-approximation.

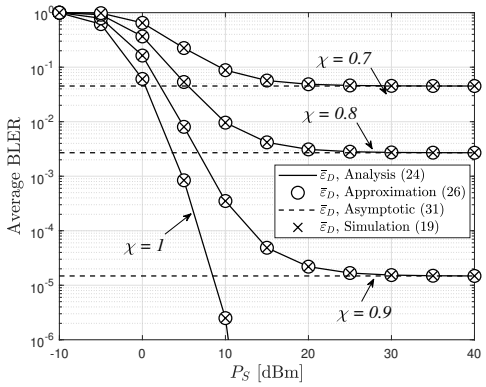

Fig. 2. Average BLER versus P_S for different values of χ with $N = 8$.

The average BLER versus P_S in dBm, both analytical and simulated, is shown in Fig. 2 for various values of χ. In addition to the imperfect CSI $(0 < \chi < 1)$, a perfect CSI $(\chi = 1)$ scenario is also included for comparison. Fig. 2 shows that in all SNR regimes, the analytical results match the simulation results. Regardless of the average BLER curve trend, we observe that there is no major calculation error between the approximated curve $\bar{\varepsilon}_D^{App}$ and the analytical one $\bar{\varepsilon}_D$ in (20). The average BLER increases when χ increases, as predicted. This occurs because a higher χ corresponds to a higher end-to-end SINR. Fig. 2 illustrates how, for the imperfect CSI scheme, fixing N and χ increases the average BLER through an increase in SNR. There is an outage floor at high SNR. The phenomena of the outage floor may be

explained as follows: (6) indicates that interference resulting from faulty CSI is favored in the numerator as the SNR grows. It should be mentioned that the asymptotic average BLERs and the outage floor values are the same. Additionally, it is discovered that the average BLER deteriorates as chi falls when $N = 8$ and $(0 < \chi \leq 1)$. This is because a lesser chi value indicates a less precise CSI.

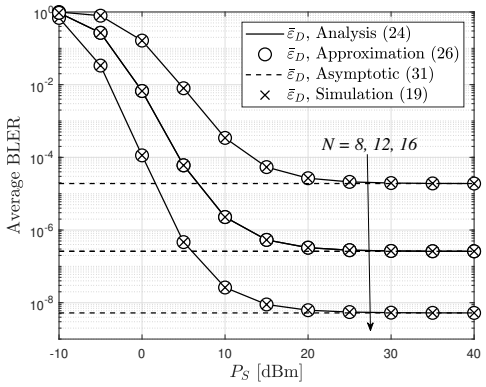

Fig. 3. Average BLER versus P_S with various number of RIS elements $N = 8, 12, 16$ and $\chi = 0.9$.

The average BLER of D vs P_S in dBm with various RIS components is displayed in Fig. 3. Those numbers show that when the P_S rises, the average BLER of D falls off significantly. Additionally, the more elements the RIS has, the better BLERs the system produces. This is because additional reflecting connections are set up to amplify received signals, which improves SINRs for the user. On the other hand, in the high-SNR zone, the average BLER performance approaches a floor when the CSI operation is imperfect.

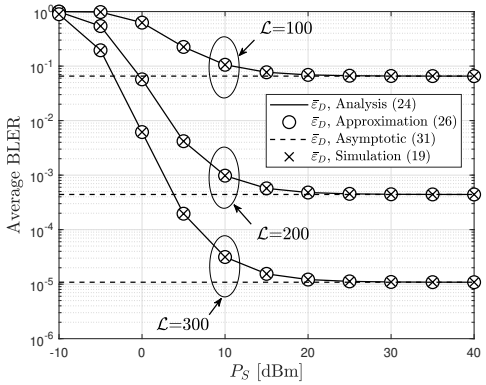

Fig. 4. Average BLER versus P_S with $N = 12$, $\chi = 0.8$ and different $\mathcal{L}$.

Alternatively, Fig. 4 depicts the average BLER of D when the blocklength $\mathcal{L}$ is varied. As seen in Fig. 4, increasing the blocklength enhances BLER performance. That is expected because the larger bocklength the system, the greater the MAR the user might receive. In other words, because the BLER has an inverse ratio with blocklength, BLER performance should improve as blocklength increases. However, this may result in increased end-to-end latency. As a result, the tradeoffs between system dependability in terms of BLER performance and system latency must be examined further.

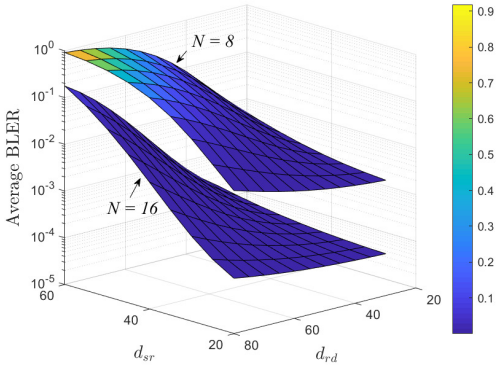

Fig. 5. Average BLER versus d_{sr} and d_{rd} with $P_S = -5$ [dBm], $\chi = 0.8$ and different N.

Fig. 5 shows the average BLER vs distance between S-RIS and RIS-D at various reflecting element counts. The average BLER of D varies substantially with distance, however, the user's average BLER performance is strong when they are closer to the base station and RIS. Furthermore, we predict that increasing the number of reflecting elements in the RIS, specifically $N = 16$, increases BLER performance.

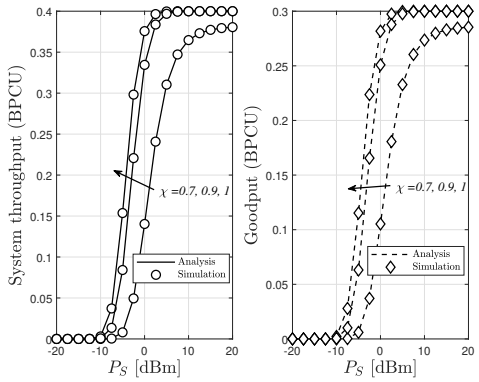

Fig. 6. System throughput/goodput comparison with $N = 8$, $\eta = 80$ bits, $calL = 200$ and different χ.

Fig. 6 shows the system throughput/goodput versus P_S in dBm for different χ values. We compare system throughput/goodput for parameter imperfect CSI. It has been shown that when transmission power and chi increase, network throughput improves. This is because a lesser χ indicates less accurate CSI. In (4), when $\chi = 0$, the first term disappears and the second term becomes the desired signal.

Finally, Fig. 7 illustrates the user's latency and reliability versus P_S in dBm. As seen in Fig. 7, the delay curves reduce dramatically as PS increases from -10 dBm to 30

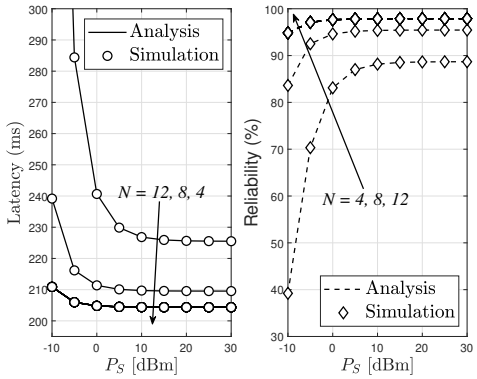

Fig. 7. Latency and reliability versus P_S with $\chi = 0.7$.

dBm. However, greater PS levels cause delay saturation. This is because a higher value of P_S results in a lower value of BLER in (33a). In example, even with a transmit power of 0 dBm, the user delay is less than 1 ms, demonstrating that our proposed system can fulfill the strict requirements for URLLC applications. In contrast to the delay trend, the reliability curves in Fig. 7 rise considerably as PS increases from -10 dBm to 30 dBm before hitting saturation. To attain 95% dependability, D requires a transmit power of 12 dBm at S and an increase of $N = 12$ reflecting elements.

V. Conclusion

The performance of an imperfect CSI of the RIS-D link in a RIS-aided SPC network was examined in this article. We obtained closed-form formulations for the average end-to-end BLER of destination, SPC, throughput, goodput, latency, and dependability. The estimated BLER of the destination is theoretically studied, as is the asymptotic BLER in a high SNR regime. Numerical findings demonstrated that the analytical results line up with simulation results, confirming the accuracy of our theoretical derivation. It is discovered that, in contrast to the ideal CSI system, inaccurate CSI results in a performance floor at high SNR, and that the floor values may be raised by adding more reflecting elements. The simulation findings provide intriguing insights into the influence of blocklength and RIS element count on the BLERs of the considered system. Furthermore, the user's performance was considerably decreased by the Imperfect CSI, demonstrating the significance of constructing an estimator circuit to lower the transmit power resource.

Appendix A
Proof of Proposition 1

From [32], $\bar{\varepsilon}_D$ is transformed as follows

$$\begin{aligned}\bar{\varepsilon}_D =& \varsigma\phi \int_0^{\infty} H\left(1-\left|\frac{x}{\varpi}\right|\right) H\left(\left|\frac{x}{\tau}\right|-1\right) \\ &\times G_{2,3}^{2,2}\left(\frac{\Xi^2 x}{\chi^2\xi}\,\middle|\, \begin{matrix}1-\varphi, 1\\ k_w, m_w, 0\end{matrix}\right) dx,\end{aligned} \tag{A.1}$$

where $H(x)$ indicates the unit step function denoted by $H(x) = \begin{cases} 1, x > 0 \\ 0, x < 0 \end{cases}$ and the integral above is set to Z.

To solve the integrals (A.1), we utilize the following transformations involving the Meijer G-function [23, Chpt. 8.4], [33]:

$$H(1-|x|) = G_{1,1}^{1,0}\left(x\,\middle|\, \begin{matrix}1\\ 0\end{matrix}\right), \tag{A.2}$$

$$H(|x|-1) = G_{1,1}^{0,1}\left(x\,\middle|\, \begin{matrix}1\\ 0\end{matrix}\right), \tag{A.3}$$

and the following connection is established by using the identity [25, Eq. (2.3)] and the connection [23, Eq. (8.3.2.21)] is displayed on the next page.

In (A.4), $\mathcal{H}_{p,q:u,v:e,f}^{m,n:s,t:i,j}(\cdot)$ stands for the extended generalized bivariate Fox H-function (EGBFHF) [25]. This function is easily assessed with mathematical tools such as Mathematica [34] and Matlab [35].

Substituting (A.3) and (A.2) into (A.1) and using (A.4) shown next top page, Z is given by (A.5).

Substituting (A.5) into (A.1), we can obtain (24).

The proof of Proposition 1 is completed.

References

[1] C.-B. Le, D.-T. Do, X. Li, Y.-F. Huang, H.-C. Chen, and M. Voznak, "Enabling noma in backscatter reconfigurable intelligent surfaces-aided systems," *IEEE Access*, vol. 9, pp. 33 782–33 795, 2021.

[2] K. Zhi, C. Pan, G. Zhou, H. Ren, M. Elkashlan, and R. Schober, "Is ris-aided massive mimo promising with zf detectors and imperfect csi?" *IEEE Journal on Selected Areas in Communications*, vol. 40, no. 10, pp. 3010–3026, 2022.

[3] M. Jung, W. Saad, and G. Kong, "Performance analysis of active large intelligent surfaces (liss): Uplink spectral efficiency and pilot training," *IEEE Transactions on Communications*, vol. 69, no. 5, pp. 3379–3394, 2021.

[4] K. P. Peppas, "Accurate closed-form approximations to generalised-k sum distributions and applications in the performance analysis of equal-gain combining receivers," *IET communications*, vol. 5, no. 7, pp. 982–989, 2011.

[5] Y. Cheng, K. H. Li, Y. Liu, K. C. Teh, and H. Vincent Poor, "Downlink and uplink intelligent reflecting surface aided networks: Noma and oma," *IEEE Transactions on Wireless Communications*, vol. 20, no. 6, pp. 3988–4000, 2021.

[6] L. Yang, F. Meng, Q. Wu, D. B. da Costa, and M.-S. Alouini, "Accurate closed-form approximations to channel distributions of ris-aided wireless systems," *IEEE Wireless Communications Letters*, vol. 9, no. 11, pp. 1985–1989, 2020.

[7] P. Fazio, M. Mehic, and M. Voznak, "Load monitoring and appliance recognition using an inexpensive, low-frequency, data-to-image, neural network, and network mobility approach for domestic iot systems," *IEEE Internet of Things Journal*, vol. 11, no. 8, pp. 13 961–13 979, 2024.

[8] B. Makki, T. Svensson, M. Coldrey, and M.-S. Alouini, "Finite block-length analysis of large-but-finite mimo systems," *IEEE Wireless Communications Letters*, vol. 8, no. 1, pp. 113–116, 2019.

[9] Z. Shi, H. Zhang, H. Wang, Y. Fu, G. Yang, X. Ye, and S. Ma, "Block error rate analysis of short-packet mobile-to-mobile communications over correlated cascaded fading channels," *IEEE Transactions on Vehicular Technology*, vol. 71, no. 4, pp. 4087–4101, 2022.

[10] P. K. Sharma, N. Sharma, S. Dhok, and A. Singh, "Ris-assisted fd short packet communication with non-linear eh," *IEEE Communications Letters*, vol. 27, no. 2, pp. 522–526, 2023.

[11] N. Arı, N. Thomos, and L. Musavian, "Performance analysis of short packet communications with multiple eavesdroppers," *IEEE Transactions on Communications*, vol. 70, no. 10, pp. 6778–6789, 2022.

$$\int_0^\infty x^{\lambda-1} G_{p,q}^{m,0}\left(\eta x \middle| \begin{matrix}\mathbf{a}_p\\ \mathbf{b}_q\end{matrix}\right) G_{p_2,q_2}^{m_2,n_2}\left(\theta x^h \middle| \begin{matrix}\mathbf{c}_{p_2}\\ \mathbf{d}_{q_2}\end{matrix}\right) G_{p_3,q_3}^{m_3,n_3}\left(\delta x^k \middle| \begin{matrix}\mathbf{e}_{p_3}\\ \mathbf{f}_{q_3}\end{matrix}\right) dx = \eta^{-\lambda} \times \mathcal{H}_{q,p:p_2,q_2:p_3,q_3}^{0,m:m_2,n_2:m_3,n_3}\left(\begin{matrix}(1-\mathbf{b}_q-\lambda;h,k)\\ (1-\mathbf{a}_p-\lambda;h,k)\end{matrix}\middle|\begin{matrix}(\mathbf{c}_{p_2},1)\\ (\mathbf{d}_{q_2},1)\end{matrix}\middle|\begin{matrix}(\mathbf{e}_{p_3},1)\\ (\mathbf{f}_{q_3},1)\end{matrix}\middle|\frac{\theta}{\eta^h},\frac{\delta}{\eta^k}\right). \tag{A.4}$$

$$\begin{aligned}\mathrm{Z} =& \int_0^\infty G_{1,1}^{1,0}\left(\frac{x}{\varpi}\middle|\begin{matrix}1\\0\end{matrix}\right) G_{2,3}^{2,2}\left(\frac{\Xi^2}{\chi^2\xi}x\middle|\begin{matrix}1-\varphi,1\\ k_w,m_w,0\end{matrix}\right) G_{1,1}^{0,1}\left(\frac{x}{\tau}\middle|\begin{matrix}1\\0\end{matrix}\right)dx\\ =&\varpi H_{1,1:2,3:1,1}^{0,1:2,2:0,1}\left(\begin{matrix}(0;1,1)\\(-1;1,1)\end{matrix}\middle|\begin{matrix}(1-\varphi,1);(1,1)\\(k_w,1);(m_w,1);(0,1)\end{matrix}\middle|\begin{matrix}(1,1)\\(0,1)\end{matrix}\middle|\frac{\varpi\Xi^2}{\chi^2\xi},\frac{\varpi}{\tau}\right).\end{aligned} \tag{A.5}$$

[12] T.-H. Vu, T.-V. Nguyen, T.-T. Nguyen, and S. Kim, "Performance analysis and deep learning design of wireless powered cognitive noma iot short-packet communications with imperfect csi and sic," *IEEE Internet of Things Journal*, vol. 9, no. 13, pp. 10 464–10 479, 2022.

[13] H. Ren, K. Wang, and C. Pan, "Intelligent reflecting surface-aided urllc in a factory automation scenario," *IEEE Transactions on Communications*, vol. 70, no. 1, pp. 707–723, 2022.

[14] L. Zhang, C. Pan, Y. Wang, H. Ren, and K. Wang, "Robust beamforming design for intelligent reflecting surface aided cognitive radio systems with imperfect cascaded csi," *IEEE Transactions on Cognitive Communications and Networking*, vol. 8, no. 1, pp. 186–201, 2022.

[15] G. Zhou, C. Pan, H. Ren, K. Wang, M. D. Renzo, and A. Nallanathan, "Robust beamforming design for intelligent reflecting surface aided miso communication systems," *IEEE Wireless Communications Letters*, vol. 9, no. 10, pp. 1658–1662, 2020.

[16] S. Hong, C. Pan, H. Ren, K. Wang, K. K. Chai, and A. Nallanathan, "Robust transmission design for intelligent reflecting surface-aided secure communication systems with imperfect cascaded csi," *IEEE Transactions on Wireless Communications*, vol. 20, no. 4, pp. 2487–2501, 2021.

[17] W. Wang, W. Ni, H. Tian, Z. Yang, C. Huang, and K.-K. Wong, "Safeguarding noma networks via reconfigurable dual-functional surface under imperfect csi," *IEEE Journal of Selected Topics in Signal Processing*, vol. 16, no. 5, pp. 950–966, 2022.

[18] S. K. Singh, K. Agrawal, K. Singh, C.-P. Li, and Z. Ding, "Noma enhanced hybrid ris-uav-assisted full-duplex communication system with imperfect sic and csi," *IEEE Transactions on Communications*, vol. 70, no. 11, pp. 7609–7627, 2022.

[19] L. Yang, J. Yang, W. Xie, M. O. Hasna, T. Tsiftsis, and M. D. Renzo, "Secrecy performance analysis of ris-aided wireless communication systems," *IEEE Transactions on Vehicular Technology*, vol. 69, no. 10, pp. 12 296–12 300, 2020.

[20] Q. Wu and R. Zhang, "Intelligent reflecting surface enhanced wireless network via joint active and passive beamforming," *IEEE Transactions on Wireless Communications*, vol. 18, no. 11, pp. 5394–5409, 2019.

[21] P. Yang, L. Luo, and J. Qin, "Outage performance of cognitive relay networks with interference from primary user," *IEEE Communications Letters*, vol. 16, no. 10, pp. 1695–1698, 2012.

[22] I. S. Gradshteyn and I. M. Ryzhik, *Table of integrals, series, and products*. Academic press, 2014.

[23] A. Prodnikov, Y. A. Brychkov, and O. Marichev, *Integrals and series. vol.3, More special functions*. Gordon and Breach Sci. Publ., New York, NY, USA, 1986.

[24] W. Yang, G. Durisi, T. Koch, and Y. Polyanskiy, "Quasi-static multiple-antenna fading channels at finite blocklength," *IEEE Transactions on Information Theory*, vol. 60, no. 7, pp. 4232–4265, 2014.

[25] P. Mittal and K. Gupta, *An integral involving generalized function of two variables*, 1972, vol. 75, no. 3.

[26] T.-H. Vu, T.-V. Nguyen, Q.-V. Pham, D. Benevides da Costa, and S. Kim, "Star-ris-enabled short-packet noma systems," *IEEE Transactions on Vehicular Technology*, vol. 72, no. 10, pp. 13 764–13 769, 2023.

[27] T.-T. T. Nguyen and X.-X. Nguyen, "Average block error rate analysis of irs-aided noma short-packet communication systems," in *2023 International Symposium on Electrical and Electronics Engineering (ISEE)*, 2023, pp. 91–96.

[28] T.-H. Vu, T.-V. Nguyen, Q.-V. Pham, D. B. da Costa, and S. Kim, "Short-packet communications for uav-based noma systems under imperfect csi and sic," *IEEE Transactions on Cognitive Communications and Networking*, vol. 9, no. 2, pp. 463–478, 2023.

[29] M. Shirvanimoghaddam, M. S. Mohammadi, R. Abbas, A. Minja, C. Yue, B. Matuz, G. Han, Z. Lin, W. Liu, Y. Li, S. Johnson, and B. Vucetic, "Short block-length codes for ultra-reliable low latency communications," *IEEE Communications Magazine*, vol. 57, no. 2, pp. 130–137, 2019.

[30] C. D. Ho, T.-V. Nguyen, T. Huynh-The, T.-T. Nguyen, D. B. da Costa, and B. An, "Short-packet communications in wireless-powered cognitive iot networks: Performance analysis and deep learning evaluation," *IEEE Transactions on Vehicular Technology*, vol. 70, no. 3, pp. 2894–2899, 2021.

[31] T. Do, G. Kaddoum, T. Nguyen, D. B. da Costa, and Z. J. Haas, "Multi-ris-aided wireless systems: Statistical characterization and performance analysis," *CoRR*, vol. abs/2104.01912, 2021. [Online]. Available: https://arxiv.org/abs/2104.01912

[32] C.-B. Le, D.-T. Do, A. Silva, W. U. Khan, W. Khalid, H. Yu, and N. D. Nguyen, "Joint design of improved spectrum and energy efficiency with backscatter noma for iot," *IEEE Access*, vol. 10, pp. 7504–7519, 2022.

[33] D.-T. Do, C.-B. Le, A. Vahid, and S. Mumtaz, "Antenna selection and device grouping for spectrum-efficient uav-assisted iot systems," *IEEE Internet of Things Journal*, vol. 10, no. 9, pp. 8014–8030, 2023.

[34] H. Lei, I. S. Ansari, G. Pan, B. Alomair, and M.-S. Alouini, "Secrecy capacity analysis over $\alpha-\mu$ fading channels," *IEEE Communications Letters*, vol. 21, no. 6, pp. 1445–1448, 2017.

[35] K. P. Peppas, "A new formula for the average bit error probability of dual-hop amplify-and-forward relaying systems over generalized shadowed fading channels," *IEEE Wireless Communications Letters*, vol. 1, no. 2, pp. 85–88, 2012.